

# Constraining the coherence scale of the interstellar magnetic field using TeV gamma-ray observations of supernova remnants

Matteo Pais,<sup>1</sup> Christoph Pfrommer,<sup>1</sup> and Kristian Ehlert<sup>1</sup>

<sup>1</sup>*Leibniz-Institut für Astrophysik Potsdam, An der Sternwarte 16, 14482 Potsdam, Germany*

(Dated: December 3, 2024)

Galactic cosmic rays are believed to be accelerated at supernova remnant (SNR) shocks. In the hadronic scenario the TeV gamma-ray emission from SNRs originates from decaying pions that are produced in collisions of the interstellar gas and cosmic rays. Using cosmic ray-magnetohydrodynamic simulations, we show that magnetic obliquity-dependent shock acceleration is able to reproduce the observed TeV gamma-ray morphology of SNRs solely by varying the magnetic morphology. This allows us to constrain the magnetic coherence scale around SN1006 and Vela Jr. to  $> 200_{-62}^{+10}$  pc and  $8.3_{-5.8}^{+15.1}$  pc, respectively.

PACS numbers: 98.38.Mz, 95.30.Qd, 98.70.Sa

*Introduction.*— SNR shocks are believed to energize Galactic cosmic rays (CRs) via diffusive shock acceleration [1]. This converts about 5 – 10% of the available kinetic energy into a non-thermal, power-law momentum distribution of CRs [2–5]. The most direct observational evidence for this is the gamma-ray emission associated with SNR at GeV and TeV energies. There are two competing models for the gamma-ray emission: in the leptonic model, CR electrons Compton upscatter interstellar radiation fields into the gamma-ray regime whereas in the hadronic model inelastic collisions between the interstellar medium (ISM) and CRs produce neutral pions that decay into gamma rays [6]. The latter process necessarily produces a kinematic spectral feature below GeV energies, as recently observed by the *Fermi* gamma-ray telescope [7]. However, the steep high-energy spectral slope raises questions whether this represents an unambiguous proof of CR ion acceleration at SNRs [8].

The high angular resolution ( $< 0.1^\circ$ ) of imaging air Cerenkov telescopes H.E.S.S., VERITAS, and MAGIC enables detailed morphological gamma-ray studies of SNRs and to separate or exclude contributions by compact sources such as pulsars. In particular, TeV gamma-ray observations have delivered a rich morphology of shell-type SNRs, ranging from the bi-lobed emission of SN1006 to the filamentary, patchy appearance of Vela Jr. The gamma-ray morphology could be the result of density inhomogeneities [9, 10] of the ambient ISM. It yet remains to be seen whether the fluctuation amplitude necessary for the observed gamma-ray patchiness does not introduce a corrugated shock surface [11] that is inconsistent with the observed spherical blast wave.

Here, we propose a different model in which the acceleration process imprints a rich gamma-ray morphology due to the global magnetic morphology [12]. Hybrid particle-in-cell simulations of non-relativistic, strong shocks show that diffusive shock acceleration of ions efficiently operates for quasi-parallel configurations (i.e., when the shock propagates along the upstream mag-

netic field or moves at a narrow angle to it) and converts around 15% of the available energy to CRs [13]. In contrast, a shock that propagates perpendicular to the magnetic field (or at a large angle to it, i.e., a quasi-perpendicular configuration) is an inefficient accelerator because charged particles are bound to gyrate around the flux-frozen magnetic field. As the magnetized plasma sweeps past the shock, so are the gyrating particles, which cannot return back upstream.

We aim at explaining the apparently disparate TeV morphologies of SNR 1006 and Vela Jr within a single physical model. To this end, we run a suite of simulations modeling a point explosion that encounters a range in magnetic field morphologies, from a homogeneous field to a mixture of homogeneous and turbulent fields to fully turbulent fields with varying coherence scales. We rescale our simulation parameters within observational limits to reproduce the observed gamma-ray flux. Comparing simulated to observed morphologies allows to constrain the magnetic coherence scale that the unperturbed ISM had before it encountered the SNR blast wave. Assuming statistical homogeneity, we thus constrain the magnetic coherence scale in the immediate vicinity of the SNR.

*Simulation setup.*—We perform our simulations with the massively parallel, adaptive moving-mesh code AREPO [27], using standard parameters for mesh regularization and an improved second-order hydrodynamic scheme with least-squares-fit gradient estimates and Runge-Kutta time integration [28]. Magnetic fields are treated with ideal magneto-hydrodynamics [29], using the Powell scheme for divergence control [30]. CRs are modelled as a relativistic fluid with a constant adiabatic index of 4/3 in a two-fluid approximation [31].

We localize and characterize shocks during the simulation [32] to inject CRs into the downstream [31] with an efficiency that depends on the upstream magnetic obliquity [12]. We adopt a maximum acceleration effi-

| SNR  | SN1006              |                          | Vela Jr.             |  |
|--|---------------------|--------------------------|----------------------|--|
|  | simulation          | observation              | simulation           | observation  |
| $E_{\text{SN}} [10^{51} \text{erg}]$   | 1.0                 | –                        | 1.0                  | –  |
| $L [\text{pc}]$  | 30                  | –                        | 25                   | –  |
| $n [\text{cm}^{-3}]$   | 0.026               | 0.02 – 0.4 [14, 15]      | 0.073                | 0.02 – 2.0 [16, 17]                                      |
| $D [\text{pc}]$  | 2110                | 1450 – 2200 [17–19]      | 400                  | 220 – 750 [20, 21]                                       |
| diameter $\theta_s [\text{deg}]$   | 0.5                 | 0.5 [22]                 | 2                    | 2 [22]   |
| diameter $d_s [\text{pc}]$   | 18.4                | 12.6 – 19.2 [22]         | 14                   | 7 – 26   |
| $v [\text{km s}^{-1}]$   | 4100                | 2890 – 4980 [23]         | 3000                 | 3000 [20]  |
| $t [\text{yrs}]$   | 1012                | 1012                     | 910                  | 680 – 4300 [20, 24]                                      |
| spectral index $\Gamma_{\text{TeV}}$   | 2.15                | $2.30 \pm 0.15$ [17, 25] | 2.11                 | $2.24 \pm 0.04_{\text{stat}} \pm 0.15_{\text{sys}}$ [16] |
| $\mathcal{F}_\gamma(> 1\text{TeV}) [10^{-12} \text{ph cm}^{-2} \text{s}^{-1}]$ | 0.39                | $0.39 \pm 0.08$ [25]     | 17.9                 | $23.4 \pm 5.6$ [26]                                      |
| $\lambda_B [\text{pc}]$  | $> 200_{-62}^{+10}$ | –                        | $8.3_{-5.8}^{+15.1}$ | –  |

TABLE I. Comparison of simulation and observational parameters:  $E_{\text{SN}}$  denotes the kinetic energy,  $L$  is the side length of the simulation box,  $n$  is the ISM number density,  $D$  is the distance to the SNR,  $\theta_s$  and  $d_s$  are the angular and proper extent of the blast wave,  $v$  denotes the shock velocity,  $t$  is the SNR age,  $\lambda_B$  is the magnetic coherence scale, and  $\mathcal{F}_\gamma$  is the gamma-ray flux.

ciency for CRs at quasi-parallel shocks of 15% that levels off to zero for quasi-perpendicular shocks [13]. We only model the dominant advective CR transport and neglect CR diffusion and streaming. This is justified since diffusively shock accelerated CRs experience efficient Bohm diffusion with a coefficient  $\kappa_{\text{Bohm}}$  at the shock [33], which implies a CR precursor ( $L_{\text{prec}}$ ) that is smaller than our grid cells,  $L_{\text{prec}} \sim \sqrt{\kappa_{\text{Bohm}} t} \sim 0.03 \text{ pc} \times (pc/10 \text{ TeV})^{1/2} (B/100 \mu\text{G})^{-1/2} (t/10^3 \text{ yr})^{1/2}$ . We neglect slow non-adiabatic CR cooling processes in comparison to the fast Sedov expansion.

Each simulation follows a point explosion that results from the deposition of  $E_{\text{SN}} = 10^{51} \text{ erg}$  in a homogeneous periodic box [31]. This leads to an energy-driven spherically-symmetric strong shock expanding in a low-pressure ISM with mean molecular weight  $\mu = 2.33$ . Our initial conditions are constructed by first generating a Voronoi mesh with randomly distributed mesh-generating points in our three-dimensional simulation box with  $200^3$  cells that we then relax via Lloyd’s algorithm [34] to obtain a glass-like configuration.

Our turbulent magnetic fields exhibit magnetic power spectra of Kolmogorov type with different coherence lengths. The three magnetic field components are treated independently so that the resulting field has a random phase. To fulfill the constraint  $\text{div} \mathbf{B} = 0$  we project out the radial field component in Fourier space. We set up a low total ISM pressure of  $0.44 \text{ eV cm}^{-3}$  and scale the field strength to an average plasma beta factor of unity. To ensure pressure equilibrium in the initial conditions, we adopt temperature fluctuations of the form  $n k_B \delta T = -\delta \mathbf{B}^2 / (8\pi)$  (for more details see reference [12]).

*Gamma-ray modelling.*—Our simulation models for the two SNRs are well described by the energy-conserving Sedov-Taylor solution [36] for the shock radius,  $r_s(t) = (E_{\text{SN}}/\alpha\rho)^{1/5} t^{2/5}$ , where  $\rho = \mu m_p n$  is the ISM mass den-

sity and  $\alpha$  is the self-similarity parameter. The solution for  $r_s$  remains self-similar even in the presence of obliquity-dependent CR acceleration [12].

We assume that the CR population follows a power-law momentum distribution and calculate the pion-decay gamma-ray emissivity [37, 38]. After line-of-sight integrating the gamma-ray emissivity and adding Gaussian noise (so that the mock map matches the observational noise properties), we convolve the maps with the observational point-spread function.

In a first step, we perform exploratory simulations with parameter choices guided by the self-similar scaling of the Sedov-Taylor solution. We find parameter combinations that approximately reproduce all observational characteristics (with box sizes  $L = 30$  and  $25 \text{ pc}$  for SN1006 and Vela Jr., respectively). Fixing the angular size and explosion energy of the SNR, and employing the self-similar property of the solution, we then re-scale the solution by slightly varying the ambient density within observational bounds to match the observed gamma-ray fluxes. The final set of parameters is reported in Table I.

To model SN1006 we assume a dominant homogeneous magnetic field that points to the top-left as supported by studies of radio polarization signatures [39]. We superpose a turbulent magnetic field with a correlation length  $\lambda_B = L = 30 \text{ pc}$  ( $\approx 0.8^\circ$  at  $D = 2.2 \text{ kpc}$ ) that contains 1/9 of the energy density of the homogeneous field. For Vela Jr. we perform a range of fully turbulent simulations with magnetic coherence lengths  $\lambda_B = L/n$  ( $n \in \{1, 2, 3, 4, 5\}$ ). We find that our simulation model with  $\lambda_B = L/3 = 8.3 \text{ pc}$  ( $\approx 1.2^\circ$  at  $0.4 \text{ kpc}$ ) statistically matches the gamma-ray maps best.

*Results.*—We present different physical properties of our simulation models for SN1006 and Vela Jr. in Fig. 1. While both simulation models adopt a constant background density, their magnetic structure differs. The

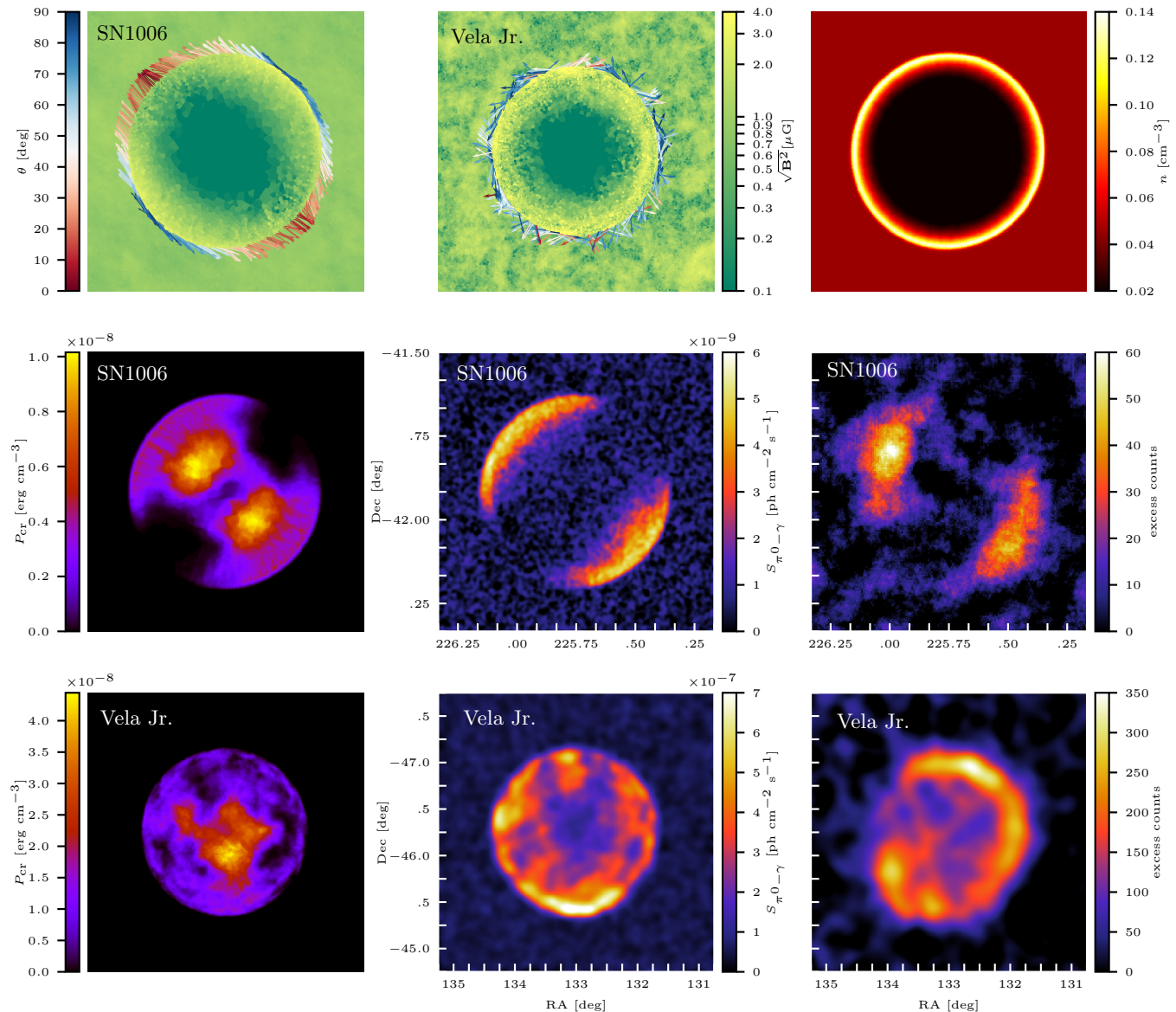


FIG. 1. Two-dimensional cross-sections and projected gamma-ray maps of our SNR simulations. Top row, left-to-right: slices of the magnetic field strengths of SN1006, Vela Jr. and of the number density  $n$ . The outwards pointing arrows in the first two panels show the orientation of the magnetic field at the shock, color-coded by the magnetic obliquity (red/blue for quasi-parallel/-perpendicular shocks). Middle row, featuring SN1006: CR pressure (left), simulated pion-decay gamma-ray surface brightness resulting from hadronic CR interactions convolved to the observational resolution (middle) and acceptance-corrected excess map for SN1006 with pixel size  $0.005^\circ$  [35]. Bottom row, featuring the same quantities for Vela Jr. with an acceptance-corrected excess map that was convolved with a Gaussian PSF of width  $\sigma = 0.08^\circ$  [26]. The simulation box of SN1006 extends to 30 pc ( $\approx 0.8^\circ$ ), that of Vela Jr. to 25 pc ( $\approx 3.6^\circ$ ). We smooth both simulated gamma-ray maps to the observational angular resolution and convolve them with Gaussian noise at the observed level. Both simulation models adopt a constant-density ISM and differ only in the assumed magnetic morphology: SN1006 has a homogeneous magnetic field pointing to the top-left augmented with a mildly turbulent field while Vela Jr. adopts a fully turbulent magnetic field with correlation length  $\lambda_B = L/3 = 8.3$  pc.

top (left and middle) panels of Fig. 1 show the magnetic field strengths of our SN1006 and Vela Jr. models augmented with the magnetic orientation at the shock (represented by arrows pointing outwards, colored according

to the magnetic obliquity: red/blue for quasi-parallel/-perpendicular shocks). The different magnetic geometry results in a significantly different CR pressure distribution owing to the obliquity-dependent shock acceleration

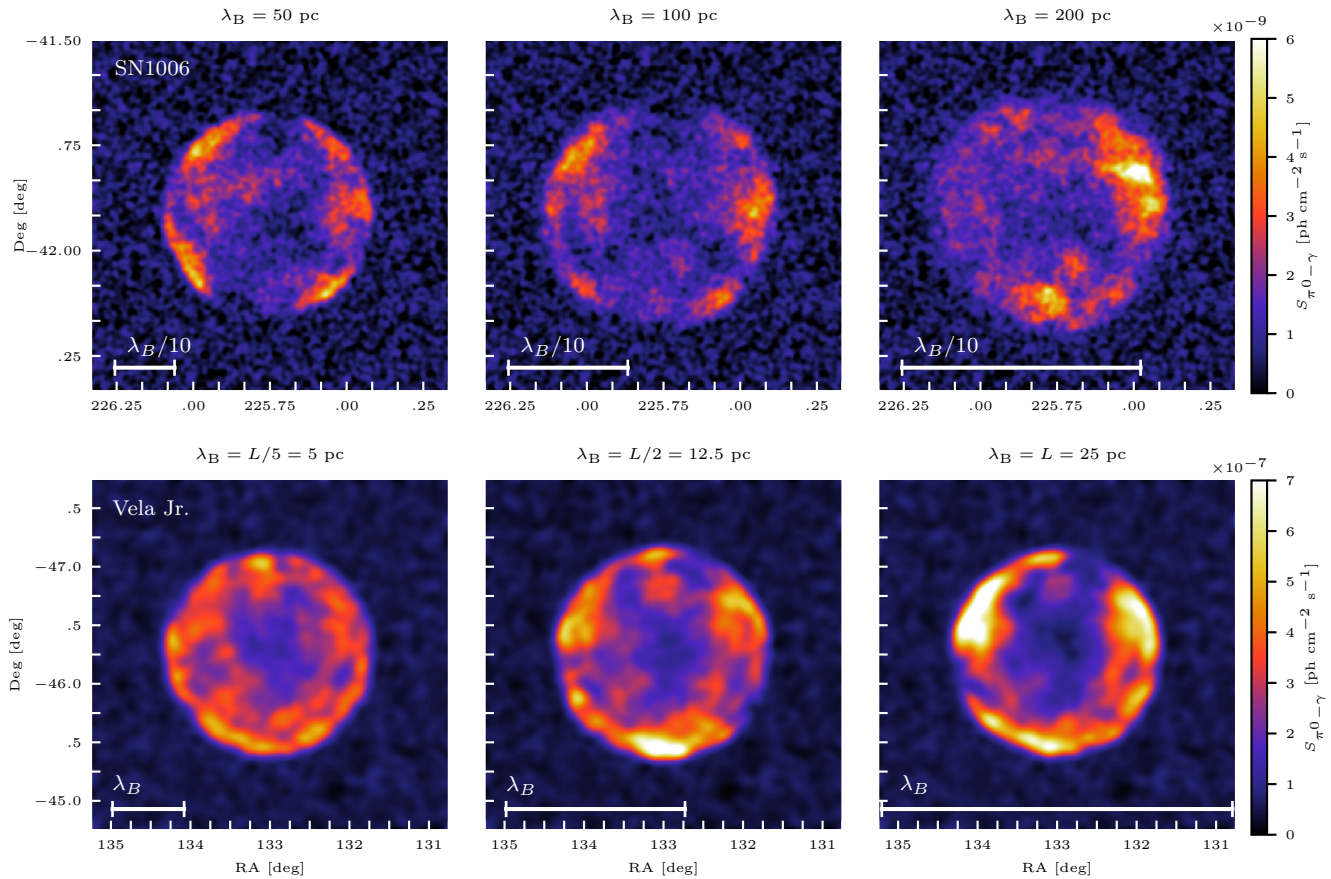


FIG. 2. Projected  $\gamma$ -ray maps of SN1006 (first row) and Vela Jr. (second row) in the case of a purely turbulent field with different coherence lengths (as indicated in the panels). The sequence towards larger correlation lengths starts to approach more homogeneous magnetic field geometries with the characteristic bi-lobed shell morphology (top right for SN1006) whereas smaller coherence lengths approach the isotropic limit (lower left for Vela Jr.). Clearly, the gamma-ray emission of Vela Jr. falls in between the cases  $\lambda_B = 5$  and  $12.5$  pc (bottom middle and right panels), justifying our choice of  $\lambda_B = 8.3$  pc.

(left column of Fig. 1, middle and bottom).

The hadronically induced gamma-ray maps echo this difference as they depend on the underlying distribution of CR pressure multiplied with the target gas density, which peaks at the shock surface (middle column of Fig. 1, middle and bottom panels). The bi-lobed gamma-ray morphology of SN1006 is a direct consequence of quasi-parallel shock configuration at the polar caps. This contrasts with the patchy filamentary, limb-brightened gamma-ray morphology of our model for Vela Jr., which results from the small-scale coherent magnetic patches with a quasi-parallel shock geometry.

A direct comparison with observational images is shown in the right column of Fig. 1, middle and bottom. In the case of SN1006, we convolve the simulated map with a Gaussian of width  $\sigma = 0.005^\circ$  (equal to the pixel size), in the case of Vela Jr. we use  $\sigma = 0.08^\circ$  (the

observational point spread function, PSF). The obliquity-dependent shock acceleration model is able to match the TeV gamma-ray morphologies of SN1006 and Vela Jr. with astonishing precision solely by changing the magnetic coherence scale (with a homogeneous field representing the limit of an infinite coherence scale). Clearly, in the case of Vela Jr. this match is on a statistical basis as the phases of turbulent fields are random. We emphasize that all our simulations assumed a constant-density ISM that the SNR has expanded into.

The success of these models enables us to estimate  $\lambda_B$  of the ISM surrounding SN1006 and Vela Jr. by comparing the observed gamma-ray maps to simulations with different values of  $\lambda_B$ . While the morphology of SN1006 is best matched by a homogeneous ambient field (possibly with the addition of a small-amplitude turbulent field), we need to perform an analysis similar to Vela Jr.

in order to formally place a lower limit on the magnetic coherence length. To this end, we perform three different simulations with a purely turbulent field that have coherence scales of  $\lambda_B = 50, 100$  and  $200$  pc.

Figure 2 shows gamma-ray maps of three different magnetic coherence scales for both SNRs, respectively. For SN1006, the number of gamma-ray patches decreases with increasing coherence scale (left to right) to the point where there are two patches visible ( $\lambda_B = 200$  pc). Since the alignment of these two patches is not symmetric with respect to the centre, we conclude that the true coherence scale must be larger and in fact is consistent with a homogeneous field across the SNR. For Vela Jr., the sequence of gamma-ray maps with decreasing coherence scale leads to smaller-scale gamma-ray patches that asymptotically approach an isotropic distribution. We find that the correlation length of Vela Jr. ranges in between the box size  $L/2$  and  $L/5$ , suggesting  $\lambda_B \approx L/3 = 8.3_{-5.8}^{+15.1}$  pc, allowing for uncertainties in distance and  $\lambda_B$ .

*Conclusions.*—We have presented the first global simulations and hadronic gamma-ray maps of SNRs, which account for magnetic obliquity-dependent CR acceleration. Our mock gamma-ray maps match the apparently disparate TeV morphologies and total gamma-ray fluxes of SNR 1006 and Vela Jr. within a single physical model extremely well: SN1006 expands into a homogeneous magnetic field that is reminiscent of conditions for a galactic outflow or a large-scale Parker loop as supported by its Galactic height of  $z = 0.53$  kpc (at  $D = 2.1$  kpc) above the midplane [40]. On the contrary, Vela Jr. is embedded in a small-scale turbulent field typical of spiral arms. This suggests that the diversity of shell-type TeV SNRs originates in the obliquity dependence of the acceleration process rather than in density inhomogeneities.

Comparing our simulations of different  $\lambda_B$  to observed TeV maps of shell-type SNRs enables us to estimate  $\lambda_B$  of the unperturbed ISM before it encountered the SNR blast wave. Assuming statistical homogeneity, we constrain  $\lambda_B$  in the vicinity of SN1006 and Vela Jr. to  $> 200_{-62}^{+10}$  pc and  $8.3_{-5.8}^{+15.1}$  pc, respectively. Our work opens up the possibility of mapping out the magnetic coherence scale across the Milky Way and other nearby galaxies at the locations of TeV shell-type SNRs, and to study how it varies depending on its vertical height or its location with respect to a spiral arm. Thus, our work represents an exciting new science case for gamma-ray astronomy, in particular for the Cherenkov Telescope Array.

*Acknowledgements.* We would like to thank the H.E.S.S. Collaboration, in particular Fabio Acero, for providing us with the published data of both SNRs. We acknowledge support by the European Research Council under ERC-CoG grant CRAGSMAN-646955.

- 
- [1] A. M. Hillas, *Journal of Physics G Nuclear Physics* **31**, R95 (2005).
  - [2] W. I. Axford, E. Leer, and G. Skadron, *International Cosmic Ray Conference* **11**, 132 (1977).
  - [3] G. F. Krymskii, *Akademiia Nauk SSSR Doklady* **234**, 1306 (1977).
  - [4] A. R. Bell, *Mon. Not. R. Astron. Soc.* **182**, 147 (1978).
  - [5] R. D. Blandford and J. P. Ostriker, *Astrophys. J. Lett.* **221**, L29 (1978).
  - [6] J. A. Hinton and W. Hofmann, *ARA&A* **47**, 523 (2009).
  - [7] M. Ackermann et al., *Science* **339**, 807 (2013).
  - [8] M. Cardillo, E. Amato, and P. Blasi, *Astron. Astrophys.* **595**, A58 (2016).
  - [9] E. G. Berezhko and H. J. Völk, *Astron. Astrophys.* **492**, 695 (2008).
  - [10] A. M. Atoyan, F. A. Aharonian, R. J. Tuffs, and H. J. Völk, *Astron. Astrophys.* **355**, 211 (2000).
  - [11] S. Ji, S. P. Oh, M. Ruszkowski, and M. Markevitch, *Mon. Not. R. Astron. Soc.* **463**, 3989 (2016).
  - [12] M. Pais, C. Pfrommer, K. Ehlert, and R. Pakmor, *ArXiv e-prints* (2018), arXiv:1805.00128 [astro-ph.HE].
  - [13] D. Caprioli and A. Spitkovski, *Astrophys. J.* **783**, 91 (2014).
  - [14] M. Miceli, S. Orlando, and V. Pereira et al., *Astron. Astrophys.* **593**, A26 (2016).
  - [15] S. Katsuda, R. Petre, K. S. Long, S. P. Reynolds, P. F. Winkler, K. Mori, and H. Tsunemi, *Astrophys. J. Lett.* **692**, L105 (2009).
  - [16] F. Aharonian et al., *Astrophys. J.* **661**, 236 (2007).
  - [17] F. Acero, M. Lemoine-Goumard, M. Renaud, J. Ballet, J. W. Hewitt, R. Rousseau, and T. Tanaka, *Astron. Astrophys.* **580**, A74 (2015).
  - [18] P. F. Winkler, G. Gupta, and K. S. Long, *Astrophys. J.* **585**, 324 (2003).
  - [19] S. Katsuda, “Supernova of 1006 (G327.6+14.6),” in *Handbook of Supernovae, Springer International Publishing AG* (2017) 1702.02054 [astro-ph.HE].
  - [20] S. Katsuda, H. Tsunemi, and K. Mori, *Astrophys. J. Lett.* **678**, L35 (2008).
  - [21] A. N. Cha, K. R. Sembach, and A. C. Danks, *Astrophys. J. Lett.* **515**, L25 (1999).
  - [22] D. A. Green, *Bulletin of the Astronomical Society of India* **42**, 47 (2014).
  - [23] F. Acero, J. Ballet, and A. Decourchelle, *Astron. Astrophys.* **475**, 883 (2007).
  - [24] A. F. Iyudin, V. Schönfelder, K. Bennett, H. Bloemen, R. Diehl, W. Hermsen, G. G. Lichti, R. D. van der Meulen, J. Ryan, and C. Winkler, *Nature (London)* **396**, 142 (1998).
  - [25] H.E.S.S. Collaboration, *Astron. Astrophys.* **516**, A62 (2010).
  - [26] H.E.S.S. Collaboration, *Astron. Astrophys.* **612**, A7 (2018).
  - [27] V. Springel, *Mon. Not. R. Astron. Soc.* **401**, 791 (2010).
  - [28] R. Pakmor, V. Springel, A. Bauer, P. Mocz, D. J. Munoz, S. T. Ohlmann, K. Schaal, and C. Zhu, *Mon. Not. R. Astron. Soc.* **455**, 1134 (2016).
  - [29] R. Pakmor and V. Springel, *Mon. Not. R. Astron. Soc.* **432**, 176 (2013).
  - [30] K. G. Powell, P. L. Roe, T. J. Linde, T. I. Gombosi, and D. L. De Zeeuw, *J. Comput. Phys.* **154**, 284 (1999).

- [31] C. Pfrommer, R. Pakmor, K. Schaal, C. M. Simpson, and V. Springel, *Mon. Not. R. Astron. Soc.* **465**, 4500 (2017).
- [32] K. Schaal and V. Springel, *Mon. Not. R. Astron. Soc.* **446**, 3992 (2015).
- [33] M. D. Stage, G. E. Allen, J. C. Houck, and J. E. Davis, *Nature Physics* **2**, 614 (2006).
- [34] S. P. Lloyd, *IEEE Trans. Information Theory* **28**, 129 (1982).
- [35] F. Acero and F. Aharonian et al., *Astron. Astrophys.* **516**, A62 (2010).
- [36] L. I. Sedov, *Similarity and Dimensional Methods in Mechanics*, New York: Academic Press (1959).
- [37] C. Pfrommer and T. A. Enßlin, *Astron. Astrophys.* **413**, 17 (2004).
- [38] C. Pfrommer, T. A. Enßlin, and V. Springel, *Mon. Not. R. Astron. Soc.* **385**, 1211 (2008).
- [39] E. M. Reynoso, J. P. Hughes, and D. A. Moffett, *Astronom. J.* **145**, 104 (2013).
- [40] F. R. Stephenson and D. A. Green, Historical supernovae and their remnants, by F. Richard Stephenson and David A. Green. International series in astronomy and astrophysics, vol. 5. Oxford: Clarendon Press, 2002, ISBN 0198507666 **5** (2002).